Aligned human induced pluripotent stem cell-derived cardiac tissue improves contractile properties through promoting unidirectional and synchronous cardiomyocyte contraction

Biomaterials 281 (2022) 121351

Contents lists available at ScienceDirect

Biomaterials

journal homepage: www.elsevier.com/locate/biomaterials

Aligned human induced pluripotent stem cell-derived cardiac tissue improves contractile properties through promoting unidirectional and synchronous cardiomyocyte contraction

Takuma Takada [a], Daisuke Sasaki [b,**], Katsuhisa Matsuura [a,b,*], Koichiro Miura [a,b], Satoru Sakamoto [a,b], Hiroshi Goto [b,c], Takashi Ohya [d], Tatsuro Iida [a,b], Jun Homma [b], Tatsuya Shimizu [b], Nobuhisa Hagiwara [a]

[a] Department of Cardiology, Tokyo Women's Medical University, Japan
[b] Institute of Advanced Biomedical Engineering and Science, Tokyo Women's Medical University, Japan
[c] Department of Cardiovascular Surgery, University of Tokyo, Japan
[d] Department of Modern Mechanical Engineering, Waseda University, Japan

ARTICLE INFO

Keywords:
Human iPSC-derived cardiomyocytes
Alignment
Contractile properties
Synchronicity

ABSTRACT

Alignment, as seen in the native myocardium, is crucial for the fabrication of functional cardiac tissue. However, it remains unclear whether the control of cardiomyocyte alignment influences cardiac function and the underlying mechanisms. We fabricated aligned human cardiac tissue using a micro-processed fibrin gel with inverted V-shaped ridges (MFG) and elucidated the effect of alignment control on contractile properties. When human induced pluripotent stem cell-derived cardiomyocytes (hiPSC-CMs) were seeded on MFG, hiPSC-CMs were aligned more uniformly than the control, and we succeeded in fabricating the aligned cardiac tissue. Assessing the contractile properties with the direct contractile measurement system, the contractile force, maximum contractile velocity, and relaxation velocity were significantly increased in aligned cardiac tissue compared with non-aligned cardiac tissue. However, gene expression profiles were not different between the two groups, suggesting that functional improvement of cardiac tissue through alignment control might not be dependent on cardiomyocyte maturation. Motion capture analysis revealed that the cardiomyocytes in the aligned cardiac tissues showed more unidirectional and synchronous contraction than the non-aligned cardiac tissues, indicating that cardiac tissue maturation involves electrical integration of cardiomyocytes. Herein, cardiomyocyte alignment control might improve the contractile properties of cardiac tissue through promoting unidirectional and synchronous cardiomyocyte contraction.

1. Introduction

Bioengineered human cardiac tissues harboring pluripotent stem cell (PSC)-derived cardiomyocytes are under development worldwide. Nevertheless, there is still an unmet need to fabricate native-like functional cardiac tissue, as PSC-derived cardiomyocytes and cardiac tissues are immature [1,2]. For example, the contractile force of native cardiac tissue was 16–44 mN/mm^2 [3,4]. On the other hand, the fabricated cardiac tissue showed 3.3 mN/mm^2 in our previous report [5]. Various strategies that enable cardiomyocyte maturation have been reported; these include long term cardiomyocyte culture [6], mechanotransduction [7], mechanical stimulation [8], cyclic stretch [9], hormonal interventions [10], and electrical stimulation [11]. In addition to cardiomyocyte maturation, cardiac tissue maturation, such as the electrical integration of cardiomyocytes, is indispensable for sufficient contractile force generation. However, it remains unclear how the cardiac tissue matures and whether contractile force is affected by tissue maturation.

The native myocardium is composed of several layers of aligned cardiac tissue, which enables efficient cardiac output [12]. Therefore, control of cardiomyocyte alignment might be a critical issue for tissue

* Corresponding author. Department of Cardiology, Tokyo Women's Medical University, Japan.
** Corresponding author. Institute of Advanced Biomedical Engineering and Science, Tokyo Women's Medical University, 8-1 Kawadacho, Shinjuku-ku, Tokyo, 162-8666, Japan.
E-mail addresses: sasaki.daisuke@twmu.ac.jp (D. Sasaki), matsuura.katsuhisa@twmu.ac.jp (K. Matsuura).

https://doi.org/10.1016/j.biomaterials.2021.121351
Received 19 September 2021; Received in revised form 17 December 2021; Accepted 27 December 2021
Available online 30 December 2021

Abbreviations

hiPSC-CM	human induced pluripotent stem cell-derived cardiomyocytes
PDMS	polydimethylsiloxane
MFG	micro-processed fibrin gel with inverted V-shaped ridges

function. Various methods have been reported for cardiomyocyte alignment in bioengineered cardiac tissue, and the improvement of contractile function has been demonstrated in aligned cardiac tissues by measuring relative displacement in local areas during tissue contraction [13–15]. However, these strategies might not be sufficient for evaluating the contractile function of the entire tissue, which is the desired functional unit. Recently, we developed a novel system to measure the real-time contractile force generated by human induced PSC-derived cardiomyocyte (hiPSC-CM) cell sheet tissues on a fibrin gel [5]. This system can directly measure contractile properties, including the systolic and relaxation functions in the entire cardiac tissue containing the base materials. However, it remains unclear whether cardiomyocyte alignment control influences cardiac contractile function and the underlying mechanisms.

In the present study, we fabricated aligned human cardiac tissue using a micro-processed fibrin gel and elucidated the effect of alignment control on contractile properties using the direct contractile measurement system in order to evaluate cell integration as tissue maturation.

2. Materials and methods

2.1. Microfabrication process

Micro V-shaped grooves with a depth of 10 μm, an angle of 54.7°, and at intervals of 30 μm, were processed on a silicon wafer by anisotropic etching (Fig. 1A); this process was outsourced to the PHOTO PRECISION Corporation (Tokyo, Japan). Next, the microfabricated silicon wafer surface was transcribed onto a cyclo olefin polymer (COP) surface by thermal imprinting (Fig. 1B); this process was outsourced to Kyodo International Inc. (Kanagawa, Japan). Reflectance confocal microscopy (OPTELICS H1200; Lasetec Corporation, Kanagawa, Japan) demonstrated that the COP surface had inverted micro V-shaped ridges with a height of 10 μm and an interval of 30 μm (Fig. 1C). The microfabricated COP surface was treated with a mixture of Novec™ 7100 and Novec™ 1700 (3 M) at a ratio of 5:1 for 30 s. Then, polydimethylsiloxane (PDMS; Silpot™ 184, Dow Corning Toray, Tokyo, Japan) was cured on the COP in a polystyrene dish at 70 °C for 120 min (Fig. 1D and E). Fig. 1F shows a microscopic image of the cross section of the resulting microfabricated PDMS surface with micro V-shaped grooves. The phase-contrast microscopic images of the microfabricated PDMS surface are shown in Fig. 1G.

2.2. Fibrin gel preparation

The fibrin gel was prepared with a minor change in the previous strategy [5]. The silicone rubber (1.5 mm thickness) with a 12 mm × 26 mm rectangular cutout was placed on the microfabricated PDMS or a normal silicone rubber to compose a mold for fibrin gel preparation. Using a 3D printer (Connex3™ Objet269; Stratasys, Eden Prairie, MN, USA), the handles were constructed, consisting of 12 mm × 8 mm × 1.4 mm thickness plates with a 6 mm × 3 mm rectangular hole and a 12 mm × 2 mm mesh on one side, made of ultraviolet-curing resin (MED610; Stratasys). The two handles were inserted into each edge of the mold, as shown in Fig. 1H. Fibrinogen (Product# F8630; Sigma-Aldrich, Missouri, USA), thrombin (Product# T4648; Sigma-Aldrich), $CaCl_2$, and lyophilized human blood coagulation factor XIII (Fibrogammin P; CSL Behring, USA) were dissolved and mixed in saline with 0.025% Polyoxyethylene (20) Sorbitan Monooleate (FUJIFILM Wako Pure Chemical, Osaka, Japan), at concentrations of 12.5 mg/mL, 0.5 units/mL, 2 mM, and more than 160 IU/mL, respectively. Immediately after mixing, the solution was poured into the mold, and an acrylic plate was placed on top (Fig. 1H and I). The solution was clotted to form a fibrin gel within 30 min. After 30 min, a micro-processed fibrin gel with inverted V-shaped ridges (MFG) or a normal surface fibrin gel (control) was prepared. The fibrin gel was picked up from the mold and inserted in 3.5 mm dishes, as shown in Fig. 1J and K. Then, the fibrin gel was immersed in Medium A [defined as DMEM (D6429; Sigma-Aldrich, Missouri, USA) containing 10% FBS and 1% Penicillin-Streptomycin Solution (P4333; Sigma-Aldrich)] with 20 μg/mL fibronectin (Corning, NY, USA) and 2.5 mg/mL aminocaproic acid (Sigma-Aldrich) for more than 2 h at 37 °C and used for seeding hiPSC-CMs, as described below. To confirm the MFG surface, we stained the fibrin gel using Flamingo™ Fluorescent Gel Stain (Bio-Rad Laboratories, CA, USA) according to the manufacturer's instructions and observed the cross-sectional plane using confocal fluorescence microscopy (FV1200; Olympus, Tokyo, Japan).

2.3. hiPSCs and cardiac differentiation

The hiPSC line 201B7 [16] was purchased from RIKEN (Tsukuba, Japan). The hiPSCs expressing α-myosin heavy chain and rex-1 promoter-driven drug-resistance genes were cultured on inactivated mouse embryonic fibroblasts (ReproCELL, Yokohama, Japan) as described previously [17]. Cardiac differentiation of hiPSCs was induced in a stirred bioreactor system (Bio Jr.8; Able, Tokyo, Japan) in accordance with a published protocol [18]. On day 17 of cardiac differentiation, cell aggregates were dissociated using 0.05% trypsin/EDTA, and the cells were cultured in medium A at 37 °C in a humidified atmosphere containing 5% CO_2 (Fig. 2A).

2.4. Purification of hiPSC-CMs and cell culture

On day 22, the culture was treated with 1.5 μg/mL puromycin (Sigma-Aldrich) for 23–25 h to eliminate non-cardiomyocytes that did not express the puromycin-resistant gene. On the next day (day 23), the cell cultures were disrupted using 0.05% trypsin/EDTA and seeded on culture dishes at a density of 1.8–2.7 × 10^5 cells/cm^2. On day 28, the cultures were again treated with 1.5 μg/mL puromycin, and, on the next day (day 29), the pure cardiomyocyte cultures were harvested using 0.05% trypsin/EDTA, following which, these cells were passed through a 40 μm nylon mesh cell strainer (Corning). Before seeding the cells, the fibrin gel was fixed in a silicon mold (Fig. 2B and F), and another thicker silicon mold with a cutout of 12 × 6 × 3 mm depth was placed on top, as shown in Fig. 2C. Thus, we seeded 2.5 × 10^5 cells in medium A containing 1% aminocaproic acid into the silicon cutout on MFG or control, as shown in Fig. 2D and G. Two days later, the silicon molds were removed carefully, and hiPSC-CMs on the fibrin gel were fixed in 3.5 cm dishes. They were immersed in medium B defined as DMEM (low glucose, GlutaMAX™ Supplement, pyruvate; Thermo Fisher Scientific, Waltham, MA, USA) containing 10% FBS, 1% penicillin-streptomycin, and 1% aminocaproic acid with extracellular matrix (Matrigel®, Corning) (Fig. 2E). From day 31, we switched the main medium from medium A to medium B until the contractile properties were evaluated. Both media A and B were replaced with fresh medium every other day. On day 41, the fabricated cardiac tissues were placed on the contractile force measurement system. We measured the contractile properties of the fabricated cardiac tissues and carried out drug tests on day 43. After measuring the properties, RNA extraction and quantitative real time polymerase chain reaction (RT-PCR) were performed on day 44 (Fig. 2A).

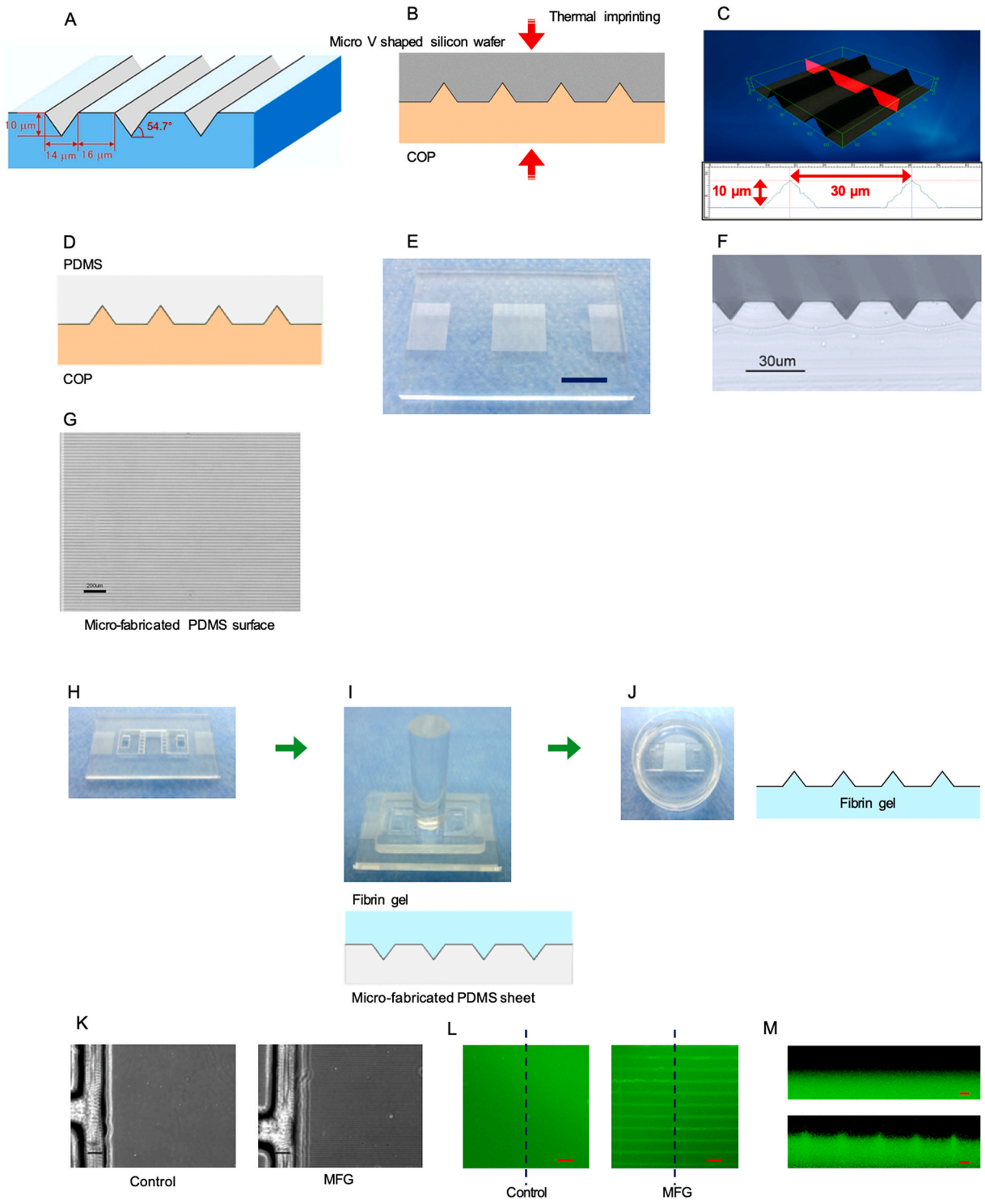

Fig. 1. Fibrin gel preparation (A) Micro-V-shaped fold of silicon wafers. One silicon wafer had 400 grooves. (B) Transcription from micro V-shaped ridge silicon wafer to COP with thermal imprinting at 100 °C. (C) Reflectance confocal microscopy image of the COP surface. (D) Transcription from micro inverted V-shaped ridge of COP to PDMS. (E) Macroscopic image of the microfabricated PDMS. Scale bar = 10 mm. (F) Microscopic image of the sectional plan of microfabricated PDMS. (G) Microscopic image of microfabricated PDMS surface. Scale bar = 200 μm. (H) Insertion of two thick plastic plates to the edge of the cutout in the silicone. (I) Fibrin gel on the microfabricated PDMS and an acrylic plate on the mold. (J) Fibrin gel picked up from the mold and inserted in 3.5 cm dishes (K) Microscopic images of the control gel (left) and MFG (right). (L) Confocal image of the control gel (left) and the MFG (right). Scale bar = 30 μm. The broken lines represent the cut lines in the sectional plan. (M) Confocal image of the sectional plan of the control (upper) and MFG (lower). Scale bar = 10 μm, COP; cyclo-olefin polymer, PDMS; polydimethylsiloxane, MFG; micro-processed fibrin gel with inverted V-shaped ridges. (For interpretation of the references to color in this figure legend, the reader is referred to the Web version of this article.)

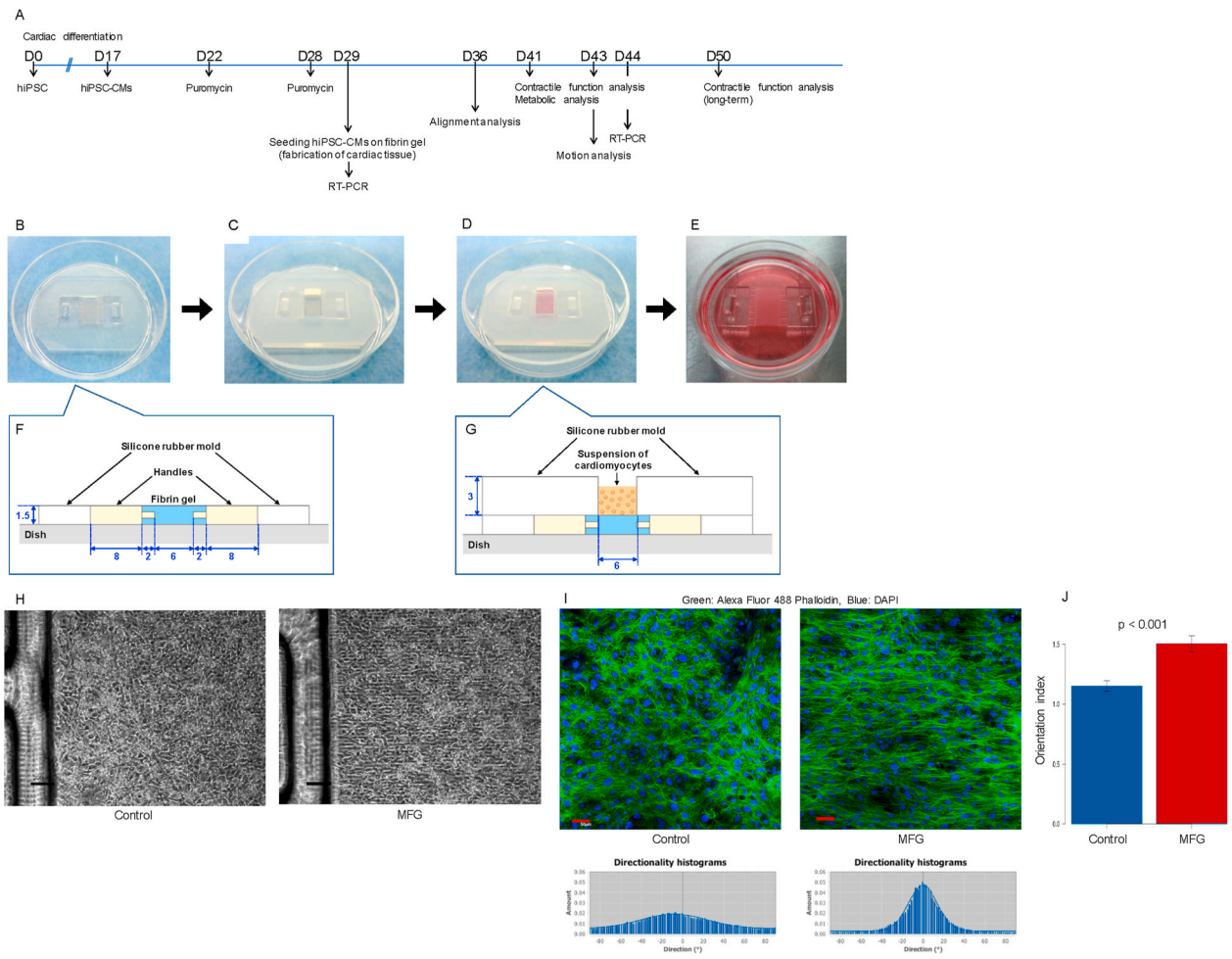

Fig. 2. Fabrication of hiPSC-CM-derived cardiac tissue (A) Time schedule of the experiments. (B) Fibrin gel fixed in silicon mold. (C) Another thicker silicon molecule is molded on the fibrin gel. (D) Seeding hiPSC-CMs on the fibrin gel in the silicon cutout. (E) hiPSC-CMs on fibrin gel fixed in a 3.5 cm dish; fabrication of hiPSC-derived cardiac tissue. (F, G) Schematic illustration of cardiomyocyte seeding on fibrin gel. All measurements were made in millimeters. (H) Microscopic images of hiPSC-CMs in the control (left) and MFG (right) on day 36 (day 7 after seeding hiPSC-CMs). Scale bar = 200 μm. (I) Confocal images of hiPSC-CMs in the control (left) and MFG (right) on day 36 (day 7 after seeding hiPSC-CMs). Scale bar = 50 μm. F-actin and nuclei were stained with Alexa Fluor 488 phalloidin and DAPI, respectively. Directionality histograms were obtained using Image J Fiji. (J) Orientation index (N = 4), hiPSC-CMs; human induced pluripotent stem cell-derived cardiomyocytes, MFG; micro-processed fibrin gel with inverted V-shaped ridges. (For interpretation of the references to color in this figure legend, the reader is referred to the Web version of this article.)

2.5. Flow cytometry

After two rounds of puromycin treatment, hiPSC-CMs were harvested and fixed with 4% paraformaldehyde. After washing with PBS, the cells were blocked with 2% bovine serum albumin (BSA, fatty acid-free, FUJIFILM Wako Pure Chemical, Osaka, Japan) prepared in PBS containing 0.2% NP40 (Nacalai Tesque, Inc., Kyoto, Japan) for 1 h. Cells were probed overnight with rabbit polyclonal anti-cardiac troponin T antibody (1:200; Abcam, Cambridge, UK) at 4 °C. On the subsequent day, the cells were washed with PBS several times and incubated with FITC-conjugated anti-rabbit antibody (Jackson ImmunoResearch Laboratories, West Grove, PA, USA). The percentage of cardiac troponin T (cTnT)-positive cells was determined using Gallios (Beckman Coulter, Brea, CA, USA) and Kaluza software (Beckman Coulter).

2.6. Contractile force measurement system

For measuring the contractile force, our previously reported contractile force measurement system was used, with slight modifications [5]. Briefly, the contractile force measurement device comprised a load cell (LVS-10GA; Kyowa Electronic Instruments, Tokyo, Japan) and a culture bath made of acrylic plates. The fabricated hiPSC-derived cardiac tissues were hung from a sensor rod in the load cell using a 3D-printed hook, and the lower handle, attached to the fibrin gel, was held by a clip on the bottom of the culture bath (Fig. 3A). Thirty five mL of medium C [defined as Medium 199, Hank's (Catalog Number 12350; Thermo Fisher Scientific) containing 10% FBS, 1% penicillin-streptomycin, and 1% aminocaproic acid] was poured into the bath. The groove direction on the fibrin gel for cardiomyocyte alignment was consistent with the direction of contractile force measurement. The contractile properties were recorded using a personal computer through an A/D converter (Power Lab 8/30; ADInstruments, Bella Vista, Australia). Electrical pacing of the fabricated cardiac tissues was conducted using bipolar platinum electrodes. Biphasic pacing pulses [10 V, 10 ms pulse duration, 60–240 paces per minute (ppm)] were applied using an electronic stimulator (Nihon Kohden, SEN-3401, Tokyo, Japan). The contractile force, maximum contractile velocity, and relaxation velocity were measured at spontaneous beat and electrical pacing rate on day 43. The time to peak contraction (TTP) and time from peak contraction to 50% relaxation (RT50) were measured at electrical pacing rate of 75 ppm and 120 ppm on day 43. Force-frequency relationship (FFR)—an index for cardiac maturation—was also measured.

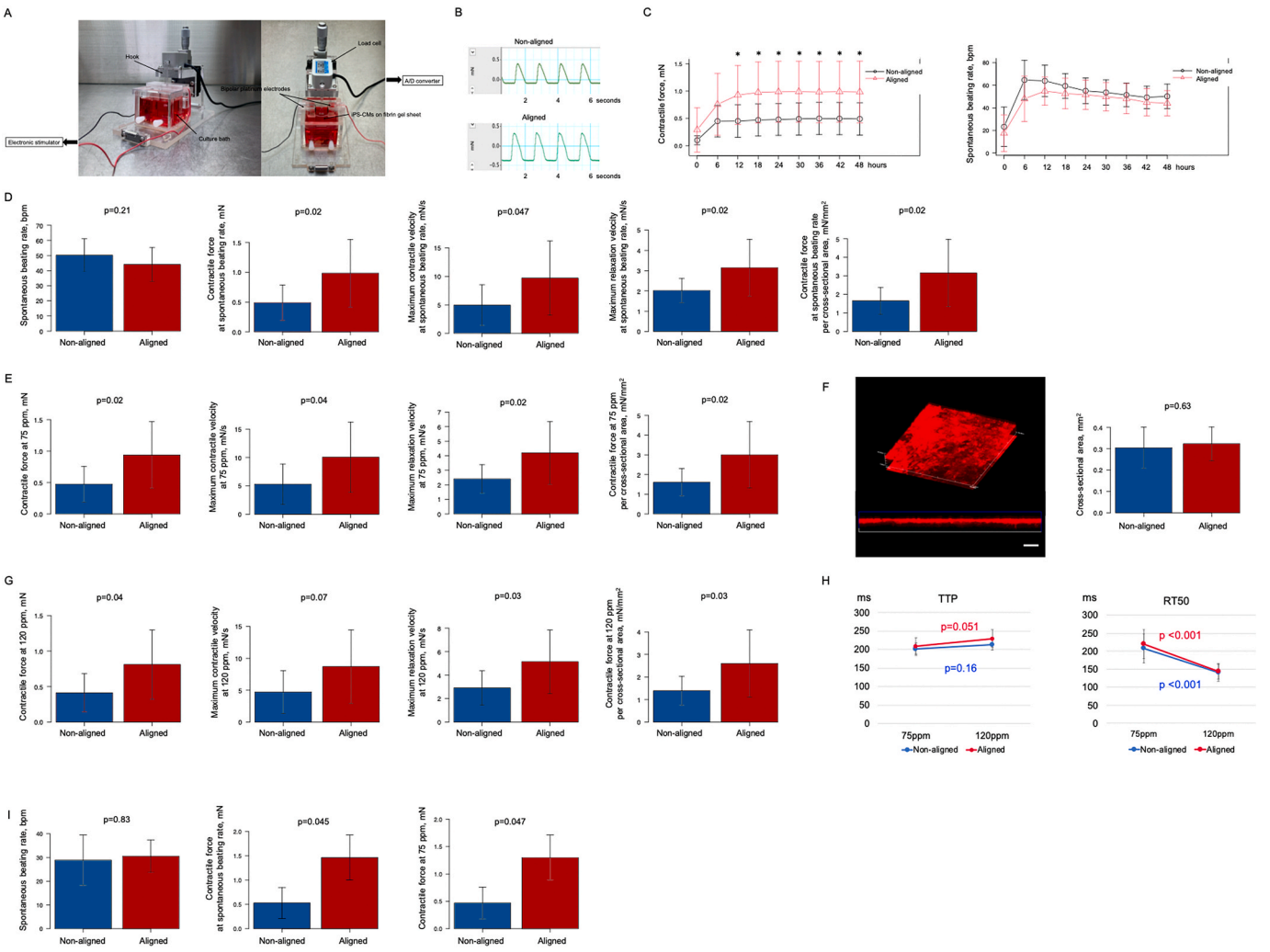

Fig. 3. Contractile force measurement system and contractile properties (A) Contractile force measurement system. (B) Representative data of contractile force trace. (C) Time course of contractile forces and spontaneous beating rates of non-aligned and aligned cardiac tissues for 48 h (N = 11). (D) Contractile properties at spontaneous beating rate (N = 11). (E) Contractile properties at 75 ppm (N = 11). (F) Cross-sectional area with confocal image (N = 11). Scale bar = 50 μm. (G) Contractile properties at 120 ppm (N = 10). (H) TTP and RT50 in the cardiac tissue at 75 ppm and 120 ppm (N = 10). (I) Contractile force and spontaneous beating rate on day 50 (N = 4), ppm; paces per minute, RT50; time from peak contraction to 50% relaxation, TTP; time to peak contraction.

To conduct drug testing, isoproterenol was added to the culture bath to fix the cardiac tissue. During the measurement of contractile force, 1 mM isoproterenol stock solution (Tokyo Chemical Industry Co., Ltd., Tokyo, Japan) was added to the culture medium (35 mL) in a culture bath, resulting in a final concentration of 1 μM. From days 41–43, the impulse was calculated for 48 h. Additionally, contractile force was measured again 1 week later (day 50) in the long-term culture.

2.7. Cell directionality analysis

To assess the orientation of the hiPSC-CMs on fibrin gel on day 36, the cells were fixed with 4% paraformaldehyde for 15 min, permeabilized with 0.15% Triton X-100 prepared in PBS, and blocked with 2% BSA prepared in PBS for 20 min at room temperature. Then, they were stained with 0.19 μM Alexa Fluor 488 Phalloidin (Thermo Fisher Scientific) at 4 °C for more than 2 h. After washing with PBS, the cells were mounted on coverslips along with anti-fade solution (ProLong Gold Antifade Reagent with DAPI; Thermo Fisher Scientific). Samples were imaged using a confocal fluorescence microscope (FV1200; Olympus, Tokyo, Japan). Images were obtained from three randomly assigned areas per sample. Cell directionality was analyzed using image processing software (ImageJ Fiji; National Institutes of Health, Bethesda, USA). The directionality histograms were analyzed using Fourier transform. Further, the orientation index of hiPSC-CMs was evaluated using FiberOri8single03 computer software by a researcher who was blinded to the type of basal fibrin gel; control or MFG group (single blind, N = 4, and a total of 12 sample images per group); if the orientation index was greater than 1.10, the alignment was clear and intense [19].

2.8. Immunohistochemistry

In some experiments, hiPSC-derived cardiac tissues were probed with mouse monoclonal *anti*-cTnT antibody (1:200, Thermo Fisher Scientific) and rabbit polyclonal *anti*-connexin43 (Cx43) antibody (1:300, Abcam), and then incubated with Alexa Fluor 488-conjugated anti-rabbit IgG (H + L) (1:200, Thermo Fisher Scientific) and Alexa Fluor 633-conjugated anti-mouse IgG (H + L) (1:200, Thermo Fisher Scientific). After staining, the cells were mounted on coverslips along with antifade solution (ProLong Gold Antifade Reagent with DAPI, Thermo Fisher Scientific). Samples were imaged using a confocal fluorescence microscope (FV1200; Olympus).

2.9. Tissue thickness and microscopic view

After measuring the contractile properties on day 43, the hiPSC-derived cardiac tissues were cultured in DMEM containing 5.6 μM CellTracker™ Orange CMTMR (Thermo Fisher Scientific) for more than 1 h, and then further cultured in DMEM for more than 1 h in a 5% CO_2 incubator at 37 °C. After fixation with 4% paraformaldehyde for 15 min, hiPSC-derived cardiac tissues were mounted on coverslips along with anti-fade solution (ProLong Gold Antifade Reagent with DAPI, Thermo Fisher Scientific). Samples were imaged using a confocal fluorescence microscope (FV1200; Olympus). The cross-sectional area and directionality histogram of hiPSC-derived cardiac tissues were analyzed using image processing software (ImageJ Fiji; National Institute of Health, Bethesda, USA). Three images from each slice were obtained per 1 sample and then averaged. When the cross-sectional areas were measured, refractive index (RI) matching was performed. The ProLong Gold Antifade Reagent with DAPI has an RI of 1.42 (https://www.thermofisher.com/order/catalog/product/S36964).

Microscopic images of hiPSC-derived cardiac tissues were obtained using an inverted microscope (ECLIPSE TI2-U; Nikon, Tokyo, Japan) equipped with a 3CCD digital camera (DXM1200C; Nikon). Microscopic videos of hiPSC-derived cardiac tissues were also obtained using an inverted microscope (ECLIPSE TE300; Nikon) equipped with a 3CCD digital camera (acA1300-30uc; Basler, Ahrensburg, Germany).

2.10. RNA extraction and quantitative RT-PCR

Total RNA was extracted from cells using an RNeasy Mini Kit (Qiagen, Hilden, Germany) according to the manufacturer's instructions. RNA quantity and quality were determined using a Nanodrop ND-1000 spectrophotometer (Thermo Fisher Scientific). First-strand cDNA was synthesized from the purified total RNA using a High Capacity cDNA Reverse Transcription Kit (Thermo Fisher Scientific) on an Applied Biosystems ProFlex™ PCR System (Thermo Fisher Scientific). Quantitative RT-PCR was performed on an Applied Biosystems® ViiA™ 7 RT-PCR system (Thermo Fisher Scientific) in accordance with the manufacturer's instructions. Gene expression levels were analyzed using TaqMan gene expression assays (Thermo Fisher Scientific) with the following primers: GAPDH, MYL2, MYL7, MYH6, MYH7, RYR2, ATP2A2, GJA1, GJA5, GJC1, PLN, CACNA1C, SCN5A, KCNH2, KCNJ2, KCNQ1, SLC8A1, SLC9A1, and NPPB (Table 1). The data were analyzed using the $\triangle$CT method. All statistical analyses were performed by comparing $\triangle$CT values between groups and were plotted as fold change ± SD ($2^{-\triangle CT}$).

2.11. Motion capture analysis of hiPSC-CMs on fibrin gel

Motion capture analyses were performed according to the following procedure. Initially, the microscopic videos of the cardiac tissue were obtained by an inverted microscope equipped with a 3CCD digital camera (acA1300-30uc; Basler). Subsequently, the moving distance to each X-axis or Y-axis of cardiomyocyte and time course at each point in the cardiac tissue were calculated using a motion analysis tool ViewPoint (Glenallan Technology Inc., Clinton, NY, USA) according to the instructions provided in the instrument manual and our previous report [20]. The maximum distances to each X- and Y-axis of the hiPSC-CMs were analyzed at the four corners over time. Furthermore, the data on time from the beginning of measurement to first peak contraction for X-axis at each point including the four corners and the center of the cardiac tissues were extracted. Then, the standard deviation of the times was calculated and compared between aligned and non-aligned cardiac tissue. When the standard deviation is smaller, the cardiomyocytes contract with more synchronous timing at each point. It means that the cardiomyocytes in the cardiac tissues perform the synchronous contraction with each other. For the analyses, the video file was converted to static images; therefore, it was compressed to 1/3 of the actual time. We additionally performed particle image velocimetry (PIV) analyses with the ImageJ plug-in PIV, which can detect the surface movement of around 4400 sites in the cardiac tissue and exhibit the movement direction and distance of each site which is approximately a cell size as an arrow. Arrows indicate the movement directions from peak relaxation phase to peak contraction phase in both type of the cardiac tissues and the color of the arrows described the movement distances of sites. Arrows with red color indicates the long movement distances of the cells compared with those with blue or purple according to the previous researches [https://sites.google.com/site/qingzongtseng/piv, [21,22]].

Table 1
PCR primer information.

Gene name	Thermo Fisher Scientific No.
glyceraldehyde-3-phosphate dehydrogenase (GAPDH)	Hs99999905_m1
myosin, light chain 2, regulatory, cardiac, slow (MYL2)	Hs00166405_m1
myosin, light chain 7, regulatory (MYL7)	Hs00221909_m1
myosin, heavy chain 6, cardiac, muscle, alpha (MYH6)	Hs01101425_m1
myosin, heavy chain 7, cardiac, muscle, beta (MYH7)	Hs01110632_m1
ATPase, Ca++ transporting, cardiac muscle, slow twitch 2 (ATP2A2)	Hs00544877_m1
ryanodine receptor 2 (cardiac) (RYR2)	Hs00181461_m1
gap junction protein, alpha 1, 43 kDa (GJA1)	Hs00748445_s1
gap junction protein alpha 5, 40 kDa (GJA5)	Hs00270952_s1
gap junction protein alpha 7, 45 kDa (GJC1)	Hs00271416_s1
phospholamban (PLN)	Hs00160179_m1
calcium channel, voltage-dependent, L type, alpha 1C subunit (CACNA1C)	Hs00167681_m1
sodium channel, voltage-gated, type V, alpha subunit (SCN5A)	Hs00165693_m1
potassium voltage-gated channel, subfamily H (eag-related), member 2 (KCNH2)	Hs00165120_m1
potassium inwardly-rectifying channel, subfamily J, member 2 (KCNJ2)	Hs00265315_m1
potassium voltage-gated channel, KQT-like subfamily, member 1 (KCNQ1)	Hs00923522_m1
potassium voltage-gated channel, shaker-related subfamily, member 2 (KCNA2)	Hs00270656_s1
potassium inwardly-rectifying channel, subfamily J, member 12 (KCNJ12)	Hs00266926_s1
solute carrier family 8 (sodium/calcium exchanger), member 1 (SLC8A1)	Hs01062258_m1
solute carrier family 9 (sodium/hydrogen exchanger), member 1 (SLC9A1)	Hs00300047_m1
natriuretic peptide B (NPPB)	Hs01057466_g1

PCR; polymerase chain reaction.

2.12. Metabolic analysis

We evaluated the change in the concentration of glucose and lactate in the culture medium during incubation for 48 h (days 41–43). The culture medium was collected on days 41 and 43, and the measurement of glucose and lactate concentrations was outsourced to SRL, Inc. (Tokyo, Japan). Impulse per glucose consumption in the cardiac tissue was calculated as the index of energy efficiency.

2.13. Statistical analysis

Continuous variables between two groups were compared using Student's *t*-test. A paired *t*-test was used to compare the contractile force, spontaneous beating rate, TTP, and RT50 between pre-isoproterenol and post-isoproterenol administration. A paired *t*-test was also used to compare TTP, and RT50 between 75 ppm and 120 ppm. A paired *t*-test was used to compare the gene expression levels between days 29 and 43 in non-aligned cardiac tissue. Significance was set at $P < 0.05$. All statistical analyses were performed using R software (version 1.41.1; R Foundation for Statistical Computing, Vienna, Austria) [23].

3. Results

3.1. Micro-processed fibrin gel

We evaluated the surface shape of the fibrin gel by staining it with Flamingo™ Fluorescent Gel Stain. The confocal image showed that there were no lines in the control gel, but lines with an interval of 30 μm were present in the MFG (Figure 1L). The cross-sectional image at the broken line shows that inverted V-shapes with a height of approximately 10 μm were observed on the MFG, and a flat surface was observed on the control fibrin gel (Figure 1M), which was consistent with the reflectance confocal microscopy image of the COP surface (Fig. 1C).

3.2. hiPSC-derived cardiac tissue preparation

After two rounds of puromycin selection, the purity of hiPSC-CMs was 89 ± 9% of cardiac troponin T (Supplementary data 1). The hiPSC-CMs were then seeded on the MFG or control fibrin gel. On day 36 (7 days after seeding hiPSC-CMs on each fibrin gel), hiPSC-CMs on MFG were aligned as shown in Fig. 2H and Supplementary Videos 1 and 2 (movie on day 37). We also evaluated the alignment of cardiomyocytes using confocal microscopy. Phalloidin staining revealed that cardiomyocytes were aligned uniformly on the MFG, but not on the control fibrin gel, as shown in Fig. 2I and Supplementary data 2. When the orientation index was calculated based on the Fourier analysis, a significantly higher orientation index was observed on MFG compared with control (1.51 ± 0.07 vs. 1.15 ± 0.05, $p < 0.001$, $N = 4$, Fig. 2J). As the orientation index of cardiomyocytes in wild type rat heart has been reported to be approximately 1.6 in our previous reports [24], cardiomyocytes on MFG might be aligned more similarly to those in the native myocardium. Furthermore, cTnT-positive cardiomyocytes and Cx43 expression were also aligned with cardiac tissue even on day 43 (14 days after seeding hiPSC-CMs on each fibrin gel, Supplementary data 3), suggesting that cardiomyocyte alignment in the dense tissue might be maintained for at least 2 weeks and that gap junctions were generated between adjacent cardiomyocytes beyond the inverted V-shaped ridge.

Supplementary data related to this article can be found online at https://doi.org/10.1016/j.biomaterials.2021.121351

3.3. Measurement of contractile properties

Next, we evaluated the influence of alignment control on contractile force using cardiac tissues on day 43 (Fig. 3A and B). Interestingly, the contractile force of the aligned cardiac tissue at the spontaneous beating rate was significantly increased compared with that of the non-aligned cardiac tissue 12 h later after fixing the cardiac tissue to the contractile force measurement system, but the spontaneous beating rate was not different between them (Fig. 3C and D). Furthermore, contractile velocity and relaxation velocity were remarkably improved in the aligned cardiac tissue (Fig. 3D). Next, we evaluated the influence of beating rate on the alignment control-mediated improvement of contractile function. Consistent with the data on the spontaneous beating rate [~50 beats per minute (bpm)], aligned cardiac tissue showed a significant improvement in contractile properties [aligned cardiac tissue vs. non-aligned cardiac tissue; contractile force at 75 ppm; 0.9 ± 0.5 mN vs. 0.5 ± 0.3 mN, $p = 0.02$, contractile velocity at 75 ppm; 10 ± 6.2 mN/s vs. 5.3 ± 3.5 mN/s, $p = 0.04$, and relaxation velocity at 75 ppm; 4.2 ± 2.1 mN/s vs. 2.4 ± 1.0 mN/s, $p = 0.02$, Fig. 3E). The aligned cardiac tissue also showed a significant improvement in contractile properties at 120 ppm, suggesting that aligned cardiac tissue might exhibit better contractile function under physiological beating rate (Fig. 3G). As the cross-sectional area was identical between the aligned and non-aligned cardiac tissues ($p = 0.63$, Fig. 3F), the contractile force per cross-sectional area was also significantly improved in the aligned cardiac tissue (Aligned vs. Non-aligned; 3.2 ± 1.8 mN/mm^2 vs. 1.7 ± 0.7 mN/mm^2 at spontaneous beating rate, $p = 0.02$, Fig. 3D–G). TTP was not significant different between 75 ppm and 120 ppm in the both types of cardiac tissue, while RT50 at 120 ppm was significantly shorter than that at 75 ppm in both types of cardiac tissue. There were no significant differences in TTP and RT50 between aligned and non-aligned cardiac tissue at 75 ppm or 120 ppm. (Fig. 3H). When these cardiac tissues were cultured for an additional week, aligned cardiac tissues still showed an improved contractile force at the spontaneous beating rate (~35 bpm) and 75 ppm upon electrical stimulation on day 50 (Fig. 3I).

3.4. Cardiomyocyte maturation evaluation

It is known that PSC-derived cardiomyocytes are immature and have insufficient function. Therefore, we examined whether alignment control results in cardiomyocyte maturation by assessing the FFR and responses against beta-adrenergic receptor agonists. As shown in Fig. 4A, the FFR was negative in the aligned and non-aligned cardiac tissues.

Treatment with isoproterenol significantly increased the spontaneous beating rate and contractile force in aligned and non-aligned cardiac tissues (Fig. 4B and C). Although the rate of increase in contractile force and contractile velocity was higher in aligned cardiac tissues than that in the non-aligned cardiac tissue (but this was not significant, $p = 0.14$ and $p = 0.17$, respectively), the rate of increase in relaxation velocity was significantly higher in aligned cardiac tissues than that in non-aligned cardiac tissues ($p = 0.007$, Fig. 4D). After isoproterenol treatment, both cardiac tissues exhibited significantly shorter TTP and RT50 compared with pre-isoproterenol treatment at 120 ppm. There were no significant differences in TTP or RT50 between aligned and non-aligned cardiac tissue in pre- or post-isoproterenol treatment (Fig. 4E).

Next, we examined the mRNA expression levels in cardiac tissues using qRT-PCR. As shown in Fig. 5, the mRNA expression levels of some contractile protein and Ca handling genes were significantly upregulated after culture, regardless of alignment. Furthermore, there were no differences in the expression levels of cardiomyocyte maturation-related genes, including ion channels between aligned and non-aligned cardiac tissues (Fig. 5 and Supplementary data 4). Herein, cardiomyocyte maturation might be promoted through the process used for tissue culture, but it might not contribute to the improvement in contractile function in aligned cardiac tissues.

3.5. Mechanisms of functional improvement in aligned cardiac tissue

First, we evaluated the movement distances at each designated point in tissues according to the X and Y axes using the motion capture analysis method (Fig. 6A and Supplementary Videos 3 and 4). The movement distance in the X-axis direction was longer in the aligned cardiac tissue than that in the non-aligned cardiac tissue (Aligned: 68 ± 26 vs. Non-aligned: 43 ± 10 μm, $p = 0.048$), but the movement distance for the Y-axis was similar between the two groups (Aligned: 27 ± 7.9 vs. Non-aligned: 33 ± 5.8 μm, $p = 0.18$). The X/Y ratio was significantly higher in the aligned cardiac tissue than that in the non-aligned cardiac tissue (Aligned: 2.5 ± 0.70 vs. Non-aligned: 1.3 ± 0.32, $p = 0.003$). Therefore, this result suggests that the aligned cardiac tissues exhibited a unidirectional contraction. Next, we examined the contraction synchronicity of each designated point in the tissues. As shown in Fig. 6B, the timing of contraction at five designated points varied in non-aligned cardiac tissue, but cells in aligned cardiac tissues showed synchronous contraction. Furthermore, the standard deviation of the time from the beginning of measurement to first peak contraction at these 5 points was significantly smaller in aligned cardiac tissues than that in the non-aligned cardiac tissue (Aligned: 0.009 ± 0.007 vs. Non-aligned: 0.03 ± 0.02 s, $p = 0.03$), suggesting that the improvement of contractile force in aligned cardiac tissue might be in part mediated by synchronous cardiomyocyte contraction.

Supplementary data related to this article can be found online at

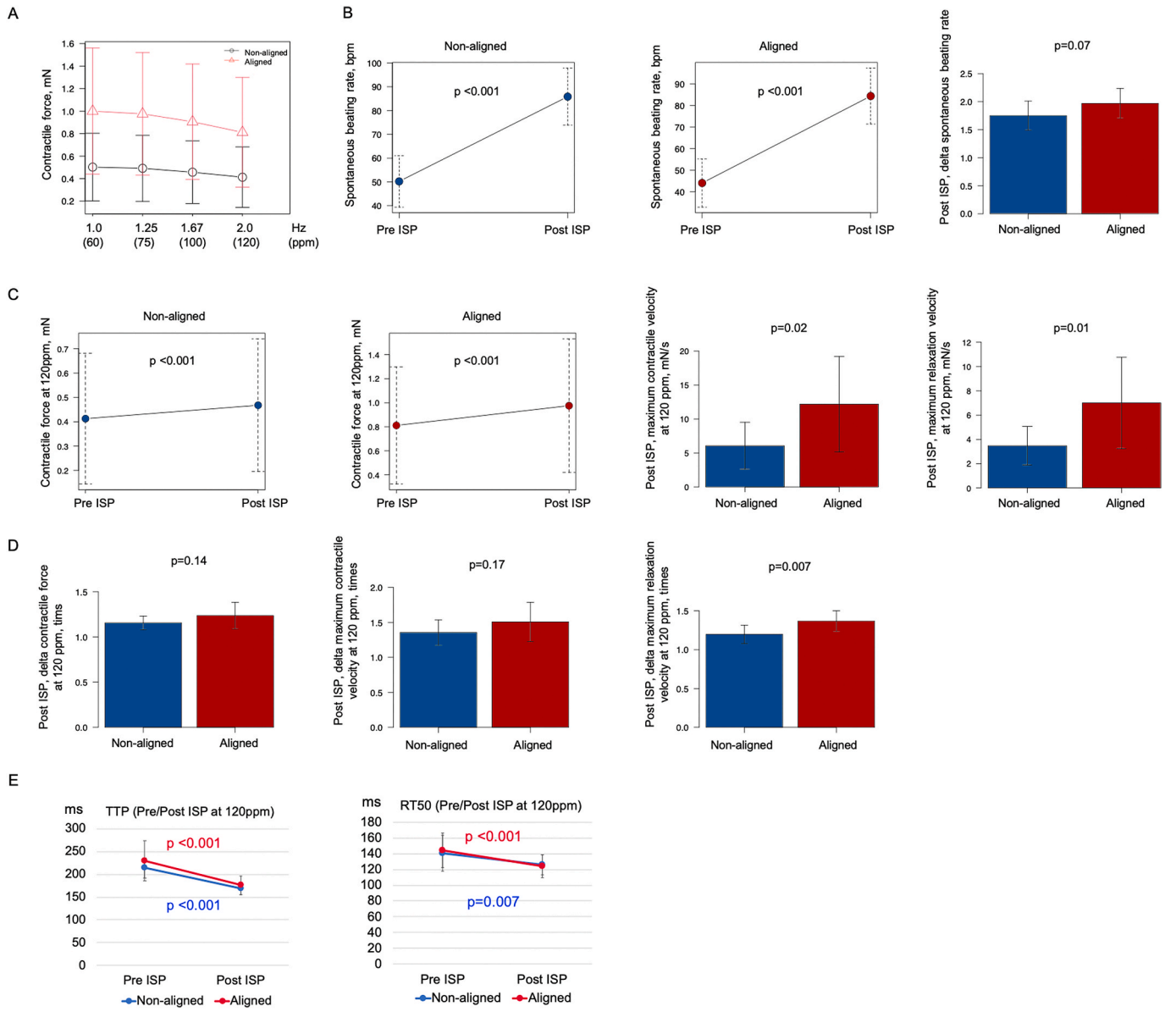

Fig. 4. Impact of isoproterenol on the aligned cardiac tissue (A) Force-frequency relationship (N = 10). (B) Spontaneous beating rate after isoproterenol administration (N = 11). (C) Contractile properties after the isoproterenol administration at 120 ppm (N = 10). (D) Changes in contractile properties after the isoproterenol administration at 120 ppm (N = 10). (E) TTP and RT50 after ISP treatment (N = 10). TTP, and RT50 at 120 ppm were same value as these factors in pre-isoproterenol at 120 ppm. ISP; isoproterenol, ppm; paces per minute, RT50; time from peak contraction to 50% relaxation, TTP; time to peak contraction.

https://doi.org/10.1016/j.biomaterials.2021.121351

Additionally, PIV analyses revealed that aligned cardiac tissue had a lot of X-axis directional arrows with red color, while non-aligned cardiac tissue had not only X-axis but also Y-axis directional arrows with non-red color (Supplementary data 5A). Vector length from peak relaxation phase to peak contraction phase at each site was significantly longer in aligned cardiac tissue compared with non-aligned cardiac tissue (Supplementary data 5B). Further, the X-axis component of the vector length was significantly longer in aligned cardiac tissue compared with non-aligned cardiac tissue (Supplementary data 5C). The sum of the X-axis component of vector length at each site was also longer in the aligned cardiac tissue than that in the non-aligned cardiac tissue (Supplementary data 5C).

3.6. Metabolic analysis

We evaluated the changes in glucose and lactate concentrations in the supernatant after incubation for 48 h. No significant differences were observed in glucose consumption and lactate production between the two groups (Fig. 7A). However, the aligned cardiac tissues had more than twice the impulse per glucose consumption of that of the non-aligned cardiac tissue (Fig. 7B). This suggests that aligned cardiac tissues generated greater contractile force with similar glucose consumption.

4. Discussion

The following were the principal findings of the present study: 1) we have succeeded in fabricating aligned hiPSC-derived cardiac tissues using the micro-processed fibrin gel, 2) the contractile properties of the aligned cardiac tissues improved compared with those of non-aligned cardiac tissues, and 3) the aligned cardiac tissue contracted with a more anisotropic, synchronized, and greater response to isoproterenol treatment for relaxation velocity than non-aligned cardiac tissue.

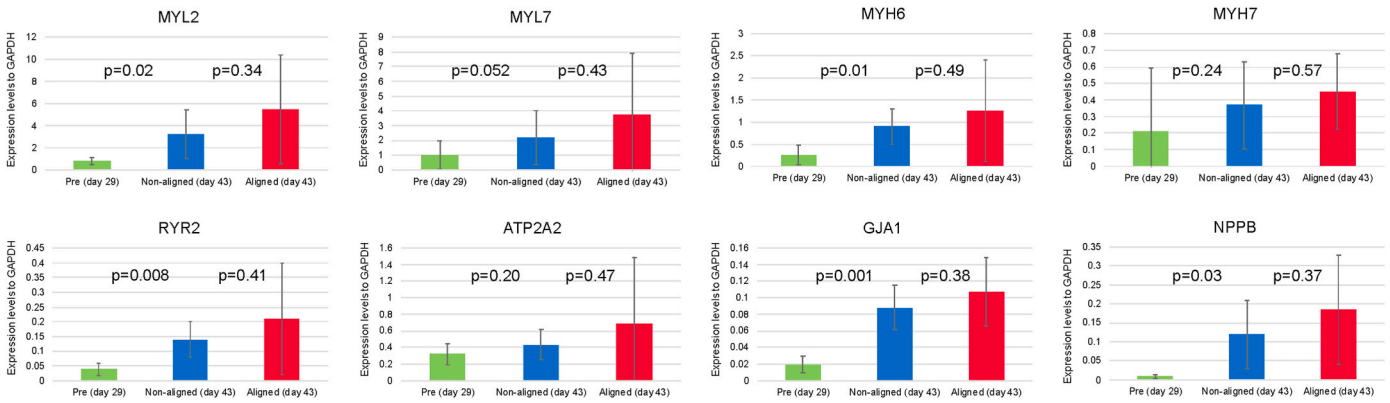

Fig. 5. Quantitative RT-PCR The P value (left side) indicates the comparison of pre- (day 29) and non-aligned cardiac tissue (day 44) (N = 6, paired *t*-test). The P value (right side) indicates the comparison of non-aligned (day 44) and aligned cardiac tissue (day 44) (N = 6, Student's t-test), RT-PCR; real time polymerase chain reaction.

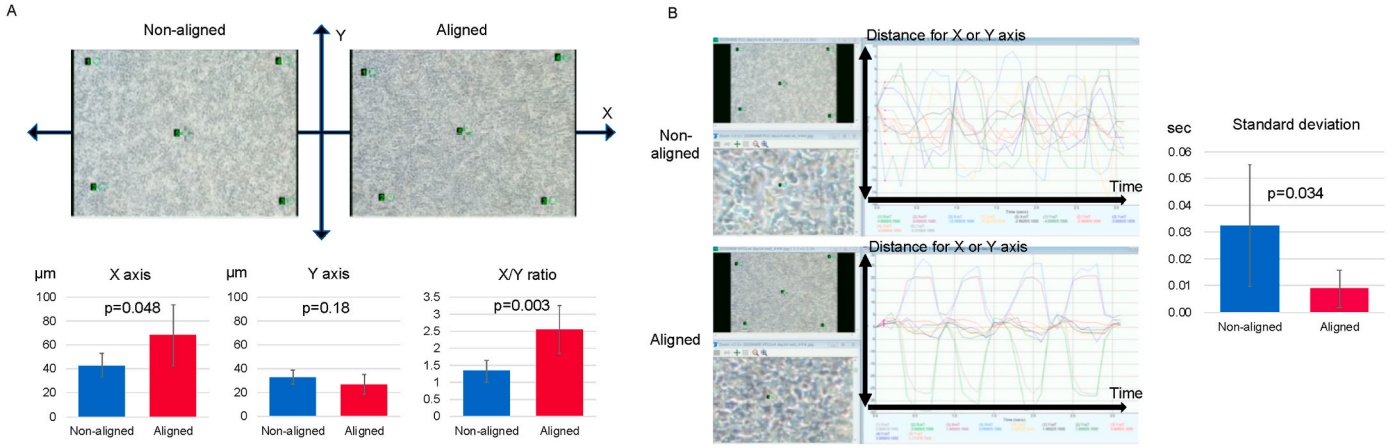

Fig. 6. Motion capture analysis of fabricated cardiac tissue (A) Motion capture image and maximum distances to the X-or Y-axis (N = 6). (B) Relationship between the distance of the X- or Y-axis and time course (left) and the standard deviation of the time from the beginning of measurement to first peak contraction to the X-axis (right) (N = 6).

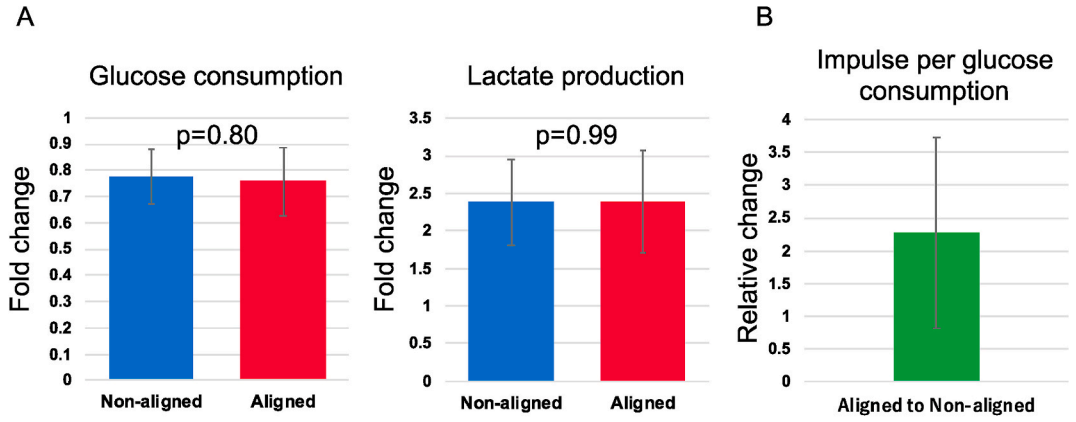

Fig. 7. Metabolic analyses (A) Metabolic change of the medium supernatant (N = 6). (B) Relative change of the impulse per glucose consumption for 48 h (N = 4).

In previous studies, aligned cardiac tissues were fabricated using nanofibers [25], PDMS [26,27], nanofiber patches [28], microfluidic systems [14], flexible thermoresponsive nanofabricated substrates [29], or decellularized tissue [15]. Then, the concepts for preparing a grooved support to fabricate aligned cardiac tissues have been previously reported [26,27,30]. Although the effect of basal materials on the cardiomyocyte contraction might be concerned, we used a soft fibrin gel as a material because Young's modulus of fibrin gel cross-linked by coagulation factor XIII is comparable to that of native human heart with little influence on cardiomyocyte contraction [31–33]. Therefore, the influence of fibrin gel on contractile force in the present study might not be critical. Several studies have reported improvements in contractile force by calculating the change in area and signal in the local imaging data [13–15,28]. However, analyzing local area movement might not be

sufficient to describe the function of the entire cardiac tissue, which is mediated not only by individual cell function, but also by cellular functional integration in tissue. We developed a contractile measurement system that can measure the contractile force of the whole cardiac tissue. Using the fibrin gel, the cardiac tissue can be fixed to the original measurement system and measured the contractile force of the whole cardiac tissue including the basal materials directly. Then, the aligned cardiac tissues showed improvement in several contractile properties, suggesting that aligned cardiac tissues had better functional properties as whole tissues. We considered that main contribution of improving the contractile force in the aligned cardiac tissue was due to the unidirectional and adequate contraction of the individual cells as well as synchronization. Motion and PIV analysis revealed that aligned cardiac tissue showed the longer movement distance in X-axis direction compared with non-aligned cardiac tissue, which might lead to the improvement of total contractile force of the tissue. The difference of the individual cardiomyocyte contractile forces and their integration between aligned and non-aligned cardiac tissue remains to be determined. Cell-to-cell connections are imperative for synchronous contraction of aligned cardiac tissue. In the present study, the micro-processed fibrin gel was designed with a height of 10 μm and an interval of 30 μm, because hiPSC-CMs had a diameter of 26 ± 17 μm ($N = 50$) (unpublished data). Furthermore, using the micro-processed fibrin gel, we succeeded in regulating hiPSC-CM alignment and in maintaining the electrical connection of hiPSC-CMs beyond the inverted V-shaped ridge (Supplementary data 3). This might have caused the synchronous contraction of hiPSC-CMs in the tissue, which contributed to the increased contractile force generated in the aligned cardiac tissue compared to that in the non-aligned cardiac tissue.

It is important to understand the similarity and differences between native myocardium and fabricated cardiac tissue. Mashali et al. showed RT50 in the native cardiac tissue decreased when the pacing rate increased [3]. The TTP and RT50 in the native cardiac tissue also decreased after isoproterenol treatment. These characteristics on kinetics might be similar between the fabricated cardiac tissue and native cardiac tissue. Conversely, contractile force of fabricated cardiac tissues is around 1/5–1/10 of native myocardium [3–5], possibly due to immaturity of PSC-derived cardiomyocytes. It has been reported that cardiac tissues from iPSC-CMs shows the lower levels of gene expression on conduction, Ca handling, and energetics than native adult heart, and systolic and relaxation function have been also improved through continuous electrical stimulation-mediated cardiomyocyte maturation [34]. In the present study, gene expression levels on contractile protein, Ca handling and ion channel were identical between aligned and non-aligned cardiac tissue. Aligned cardiac tissues also show negative FFR. Herein, cardiomyocyte maturation might not be directly attributed to the functional improvement of the aligned cardiac tissue. The fabrication of cardiac tissue through the adequate extracellular matrix (ECM) and the continuous electrical stimulation might be necessary for promoting cellular maturation [35]. On the other hand, alignment control improved the contractile properties in accompanied with the synchronous contraction. On the basis of these findings, we believe that alignment control promotes tissue maturation as electrical integration of cardiomyocytes. Native myocardium of atria or ventricle behaves as an electrically continuous sheet [12]. It has also been reported that hiPSC-CMs in cell aggregates show synchronous contraction in a time-dependent manner, accompanied by Cx43 upregulation [36]. Conversely, as Cx43 mRNA expression levels were not different between aligned and non-aligned cardiac tissues (Fig. 5), Cx43 transcriptional levels might not be critical for alignment control-mediated synchronous contraction. Cx43 is phosphorylated in the normal heart, and dephosphorylated in the ischemic heart [37], where disturbances in alignment and electrical connection occur in the cardiomyocytes. In addition, Eps15 homology domain-containing protein 1 (EHD1) was related to the endocytic trafficking of Cx43 and pathological remodeling of gap junctions under ischemic conditions [38]. Accordingly, post-transcriptome regulation of Cx43 might contribute to the synchronous contraction of cardiomyocytes in the aligned cardiac tissue.

Comparison with the contractile function in pre- and post-isoproterenol treatment in the current study, the rate of increase in relaxation velocity was significantly higher in aligned cardiac tissues than that in non-aligned cardiac tissues (Fig. 4D). G. Jung et al. demonstrated that phosphorylation of phospholamban in aligned iPSC-CMs on microgrooved PDMS was accelerated after isoproterenol treatment [26]. We considered that a modified phosphorylation profile of several relaxation related proteins including phospholamban might be associated with the rate of increase in relaxation function of aligned cardiac tissue after isoproterenol treatment as the underlying mechanism. Understanding the molecular mechanism of the alignment control-mediated synchronous contraction and response to β-stimulation might provide us the new insights on heart homeostasis and heart failure.

Although drug development and drug toxicity evaluation using iPSC-derived cardiac tissue have progressed, some problems in terms of cost and function remain. In our previous study, a contractile force of 1 mN was generated from 4.3×10^5 cells [5]. Meanwhile, the aligned cardiac tissue in the current study demonstrated that a contractile force of 1 mN could be generated from 2.5×10^5 cells. Therefore, the cost required for hiPSC-CMs to generate a similar contractile force could be reduced. Additionally, more functional cardiac tissues are ideal for drug toxicity evaluation. Aligned cardiac tissues improve the contractile force and synchronicity of cardiomyocytes, while non-aligned cardiac tissue can result in dyssynchronous and weak contractions. Further, previous reports have mainly indicated the improvement in systolic function of aligned cardiac tissue [13–15,28], while aligned cardiac tissue in the present study showed an improvement in both systolic and relaxation function. Therefore, the evaluation of drug-related cardiotoxicity including systolic and relaxation function with aligned cardiac tissue might be more appropriate than that with non-aligned cardiac tissue.

Taken together, the aligned cardiac tissue using micro-processed fibrin gel improved contractile functions through promoting unidirectional and electrical synchronicity. The use of advanced cardiac tissues is expected in regenerative therapy, drug development, and disease research, as well as to clarify the molecular mechanisms of cardiac tissue maturation through synchronous contraction.

5. Conclusions

Using the micro-processed fibrin gel, hiPSC-CMs were oriented on a fibrin gel with increased contractile properties due to synchronized anisotropic contraction without increasing glucose consumption. This might lead to the development of more functional cardiac tissue models for disease research, drug development, and regenerative therapy.

Credit author statement

Takuma Takada: Conceptualization, Methodology, Investigation, Data curation, Formal analysis, Funding acquisition, Writing – original draft. **Daisuke Sasaki:** Conceptualization, Methodology, Project administration, Writing- Reviewing and Editing, **Katsuhisa Matsuura:** Conceptualization, Methodology, Project administration, Funding acquisition, Writing- Reviewing and Editing. **Koichiro Miura:** Validation, Visualization. **Satoru Sakamoto:** Validation; Visualization. **Hiroshi Goto:** Validation, Visualization. **Takashi Ohya:** Resources, Software, Formal analysis. **Tatsuro Iida:** Resources, Software, Formal analysis. **Jun Homma:** Resources, Software, Formal analysis. **Tatsuya Shimizu:** Funding acquisition, Writing- Reviewing and Editing. **Nobuhisa Hagiwara:** Supervision.

Data availability

The data that support the finding of this study are available from the

corresponding authors upon reasonable request.

Declaration of competing interest

The authors declare the following financial interests/personal relationships which may be considered as potential competing interests: Katsuhisa Matsuura and Tatsuya Shimizu are the inventors of bioreactor systems. Tokyo Women's Medical University is funded by Nihon Kohden. The other authors declare no conflicts of interest.

Acknowledgements

We thank K. Sugiyama and M. Tejima for their excellent technical assistance. This research was supported by AMED, Japan (grant number: 20mk0104117h0403). This study was funded by a research grant from the Miyata Cardiac Research Promotion Foundation, Japan, the Kurata Grants 2020 of The Hitachi Global Foundation, Japan, SENSHIN Medical Research Foundation, Japan, and The Cardiovascular Research Fund, Japan. We would like to thank Editage (www.editage.jp) for English language editing.

Appendix A. Supplementary data

Supplementary data to this article can be found online at https://doi.org/10.1016/j.biomaterials.2021.121351.

References

[1] T.J. Kolanowski, C.L. Antos, K. Guan, Making human cardiomyocytes up to date: derivation, maturation state and perspectives, Int. J. Cardiol. 241 (2017) 379–386.
[2] E. Karbassi, A. Fenix, S. Marchiano, N. Muraoka, K. Nakamura, X. Yang, C. E. Murry, Cardiomyocyte maturation: advances in knowledge and implications for regenerative medicine, Nat. Rev. Cardiol. 17 (6) (2020) 341–359.
[3] M.A. Mashali, N.S. Saad, B.D. Canan, M.T. Elnakish, N. Milani-Nejad, J.H. Chung, E.J. Schultz, S.A. Kiduko, A.W. Huang, A.N. Hare, K.K. Peczkowski, F. Fazlollahi, B. L. Martin, J.D. Murray, C.M. Campbell, A. Kilic, B.A. Whitson, N.A. Mokadam, P. J. Mohler, P.M.L. Janssen, Impact of etiology on force and kinetics of left ventricular end-stage failing human myocardium, J. Mol. Cell. Cardiol. 156 (2021) 7–19.
[4] G. Hasenfuss, L.A. Mulieri, E.M. Blanchard, C. Holubarsch, B.J. Leavitt, F. Ittleman, N.R. Alpert, Energetics of isometric force development in control and volume-overload human myocardium. Comparison with animal species, Circ. Res. 68 (3) (1991) 836–846.
[5] D. Sasaki, K. Matsuura, H. Seta, Y. Haraguchi, T. Okano, T. Shimizu, Contractile force measurement of human induced pluripotent stem cell-derived cardiac cell sheet-tissue, PLoS One 13 (5) (2018), e0198026.
[6] T. Kamakura, T. Makiyama, K. Sasaki, Y. Yoshida, Y. Wuriyanghai, J. Chen, T. Hattori, S. Ohno, T. Kita, M. Horie, S. Yamanaka, T. Kimura, Ultrastructural maturation of human-induced pluripotent stem cell-derived cardiomyocytes in a long-term culture, Circ. J. 77 (5) (2013) 1307–1314.
[7] S. Martewicz, E. Serena, S. Zatti, G. Keller, N. Elvassore, Substrate and mechanotransduction influence SERCA2a localization in human pluripotent stem cell-derived cardiomyocytes affecting functional performance, Stem Cell Res. 25 (2017) 107–114.
[8] N.L. Tulloch, V. Muskheli, M.V. Razumova, F.S. Korte, M. Regnier, K.D. Hauch, L. Pabon, H. Reinecke, C.E. Murry, Growth of engineered human myocardium with mechanical loading and vascular coculture, Circ. Res. 109 (1) (2011) 47–59.
[9] W. Zhang, C.W. Kong, M.H. Tong, W.H. Chooi, N. Huang, R.A. Li, B.P. Chan, Maturation of human embryonic stem cell-derived cardiomyocytes (hESC-CMs) in 3D collagen matrix: effects of niche cell supplementation and mechanical stimulation, Acta Biomater. 49 (2017) 204–217.
[10] S.S. Parikh, D.J. Blackwell, N. Gomez-Hurtado, M. Frisk, L. Wang, K. Kim, C. P. Dahl, A. Fiane, T. Tonnessen, D.O. Kryshtal, W.E. Louch, B.C. Knollmann, Thyroid and glucocorticoid hormones promote functional T-tubule development in human-induced pluripotent stem cell-derived cardiomyocytes, Circ. Res. 121 (12) (2017) 1323–1330.
[11] A.F. Godier-Furnemont, M. Tiburcy, E. Wagner, M. Dewenter, S. Lammle, A. El-Armouche, S.E. Lehnart, G. Vunjak-Novakovic, W.H. Zimmermann, Physiologic force-frequency response in engineered heart muscle by electromechanical stimulation, Biomaterials 60 (2015) 82–91.
[12] N. Herring, D.J. Paterson, Levick's Introduction to Cardiovascular Physiology, sixth ed., CRC Press, FL, 2018.
[13] M. Wanjare, L. Hou, K.H. Nakayama, J.J. Kim, N.P. Mezak, O.J. Abilez, E. Tzatzalos, J.C. Wu, N.F. Huang, Anisotropic microfibrous scaffolds enhance the organization and function of cardiomyocytes derived from induced pluripotent stem cells, Biomater Sci 5 (8) (2017) 1567–1578.
[14] T.J. Kolanowski, M. Busek, M. Schubert, A. Dmitrieva, B. Binnewerg, J. Poche, K. Fisher, F. Schmieder, S. Grunzner, S. Hansen, A. Richter, A. El-Armouche, F. Sonntag, K. Guan, Enhanced structural maturation of human induced pluripotent stem cell-derived cardiomyocytes under a controlled microenvironment in a microfluidic system, Acta Biomater. 102 (2020) 273–286.
[15] A. Blazeski, J. Lowenthal, R. Zhu, J. Ewoldt, K.R. Boheler, L. Tung, Functional properties of engineered heart slices incorporating human induced pluripotent stem cell-derived cardiomyocytes, Stem Cell Reports 12 (5) (2019) 982–995.
[16] K. Takahashi, S. Yamanaka, Induction of pluripotent stem cells from mouse embryonic and adult fibroblast cultures by defined factors, Cell 126 (4) (2006) 663–676.
[17] K. Matsuura, H. Seta, Y. Haraguchi, K. Alsayegh, H. Sekine, T. Shimizu, N. Hagiwara, K. Yamazaki, T. Okano, TRPV-1-mediated elimination of residual iPS cells in bioengineered cardiac cell sheet tissues, Sci. Rep. 6 (2016) 21747.
[18] K. Matsuura, M. Wada, T. Shimizu, Y. Haraguchi, F. Sato, K. Sugiyama, K. Konishi, Y. Shiba, H. Ichikawa, A. Tachibana, U. Ikeda, M. Yamato, N. Hagiwara, T. Okano, Creation of human cardiac cell sheets using pluripotent stem cells, Biochem. Biophys. Res. Commun. 425 (2) (2012) 321–327.
[19] T. Enomae, Y.H. Han, A. Isogai, Nondestructive determination of fiber orientation distribution of paper surface by image analysis, Nord. Pulp Pap Res. J. 21 (2) (2006) 253–259.
[20] H. Takahashi, T. Shimizu, T. Okano, Engineered human contractile myofiber sheets as a platform for studies of skeletal muscle physiology, Sci. Rep. 8 (1) (2018) 13932.
[21] Q. Tseng, E. Duchemin-Pelletier, A. Deshiere, M. Balland, H. Guillou, O. Filhol, M. Thery, Spatial organization of the extracellular matrix regulates cell-cell junction positioning, Proc. Natl. Acad. Sci. U. S. A. 109 (5) (2012) 1506–1511.
[22] Y. Tsukamoto, T. Akagi, M. Akashi, Vascularized cardiac tissue construction with orientation by layer-by-layer method and 3D printer, Sci. Rep. 10 (1) (2020) 5484.
[23] Y. Kanda, Investigation of the freely available easy-to-use software 'EZR' for medical statistics, Bone Marrow Transplant. 48 (3) (2013) 452–458.
[24] J. Homma, S. Shimizu, H. Sekine, K. Matsuura, T. Shimizu, A novel method to align cells in a cardiac tissue-like construct fabricated by cell sheet-based tissue engineering, J Tissue Eng Regen Med 14 (7) (2020) 944–954.
[25] M. Ding, H. Andersson, S. Martinsson, A. Sabirsh, A. Jonebring, Q.D. Wang, A. T. Plowright, L. Drowley, Aligned nanofiber scaffolds improve functionality of cardiomyocytes differentiated from human induced pluripotent stem cell-derived cardiac progenitor cells, Sci. Rep. 10 (1) (2020) 13575.
[26] G. Jung, G. Fajardo, A.J. Ribeiro, K.B. Kooiker, M. Coronado, M. Zhao, D.Q. Hu, S. Reddy, K. Kodo, K. Sriram, P.A. Insel, J.C. Wu, B.L. Pruitt, D. Bernstein, Time-dependent evolution of functional vs. remodeling signaling in induced pluripotent stem cell-derived cardiomyocytes and induced maturation with biomechanical stimulation, Faseb. J. 30 (4) (2016) 1464–1479.
[27] C. Rao, T. Prodromakis, L. Kolker, U.A. Chaudhry, T. Trantidou, A. Sridhar, C. Weekes, P. Camelliti, S.E. Harding, A. Darzi, M.H. Yacoub, T. Athanasiou, C. M. Terracciano, The effect of microgrooved culture substrates on calcium cycling of cardiac myocytes derived from human induced pluripotent stem cells, Biomaterials 34 (10) (2013) 2399–2411.
[28] Y.D. Lin, M.C. Ko, S.T. Wu, S.F. Li, J.F. Hu, Y.J. Lai, H.I. Harn, I.C. Laio, M.L. Yeh, H.I. Yeh, M.J. Tang, K.C. Chang, F.C. Su, E.I. Wei, S.T. Lee, J.H. Chen, A. S. Hoffman, W.T. Wu, P.C. Hsieh, A nanopatterned cell-seeded cardiac patch prevents electro-uncoupling and improves the therapeutic efficacy of cardiac repair, Biomater Sci 2 (4) (2014) 567–580.
[29] N.P. Williams, M. Rhodehamel, C. Yan, A.S.T. Smith, A. Jiao, C.E. Murry, M. Scatena, D.H. Kim, Engineering anisotropic 3D tubular tissues with flexible thermoresponsive nanofabricated substrates, Biomaterials 240 (2020) 119856.
[30] B.C. Isenberg, Y. Tsuda, C. Williams, T. Shimizu, M. Yamato, T. Okano, J.Y. Wong, A thermoresponsive, microtextured substrate for cell sheet engineering with defined structural organization, Biomaterials 29 (17) (2008) 2565–2572.
[31] F.M. Shaikh, A. Callanan, E.G. Kavanagh, P.E. Burke, P.A. Grace, T. M. McGloughlin, Fibrin: a natural biodegradable scaffold in vascular tissue engineering, Cells Tissues Organs 188 (4) (2008) 333–346.
[32] P.A. Janmey, J.P. Winer, J.W. Weisel, Fibrin gels and their clinical and bioengineering applications, J. R. Soc. Interface 6 (30) (2009) 1–10.
[33] A.M. Handorf, Y. Zhou, M.A. Halanski, W.J. Li, Tissue stiffness dictates development, homeostasis, and disease progression, Organogenesis 11 (1) (2015) 1–15.
[34] K. Ronaldson-Bouchard, S.P. Ma, K. Yeager, T. Chen, L. Song, D. Sirabella, K. Morikawa, D. Teles, M. Yazawa, G. Vunjak-Novakovic, Advanced maturation of human cardiac tissue grown from pluripotent stem cells, Nature 556 (7700) (2018) 239–243.
[35] Y. Guo, W.T. Pu, Cardiomyocyte maturation: new phase in development, Circ. Res. 126 (8) (2020) 1086–1106.
[36] J. Aoyama, K. Homma, N. Tanabe, S. Usui, Y. Miyagi, K. Matsuura, M. Kaneda, T. Nitta, Spatiotemporal imaging documented the maturation of the cardiomyocytes from human induced pluripotent stem cells, J. Thorac. Cardiovasc. Surg. 159 (6) (2020) 2260–2271 e7.
[37] L. Marquez-Rosado, J.L. Solan, C.A. Dunn, R.P. Norris, P.D. Lampe, Connexin43 phosphorylation in brain, cardiac, endothelial and epithelial tissues, Biochim. Biophys. Acta 1818 (8) (2012) 1985–1992.
[38] T. Martins-Marques, S. Catarino, A. Goncalves, D. Miranda-Silva, L. Goncalves, P. Antunes, G. Coutinho, A. Leite Moreira, I. Falcao Pires, H. Girao, EHD1 modulates Cx43 gap junction remodeling associated with cardiac diseases, Circ. Res. 126 (10) (2020) e97–e113.

Supplementary Materials

Supplementary data 1. Purity of hiPSC-CMs after two rounds of puromycin treatment

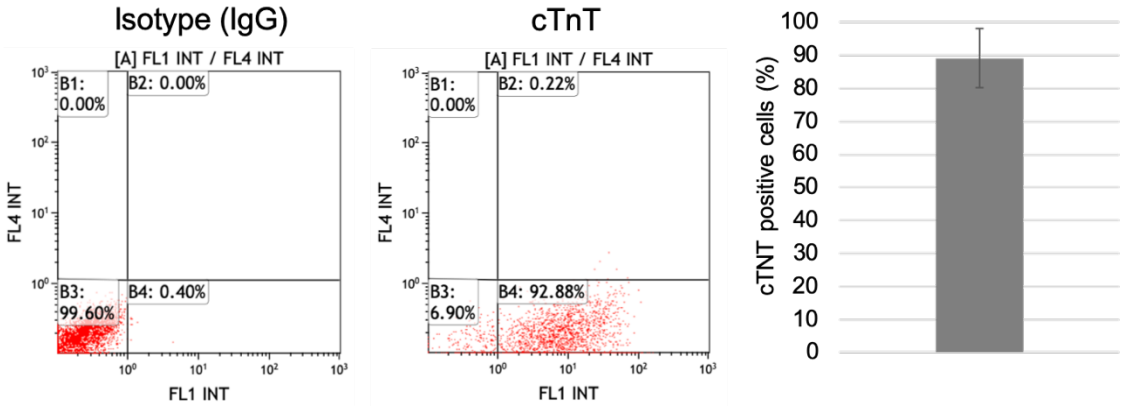

The purity of hiPSC-CMs was 89 ± 9% of cardiac troponin T (n =3).

Supplementary data 2. Confocal images of hiPSC-CMs in the control (left) and MFG (right)

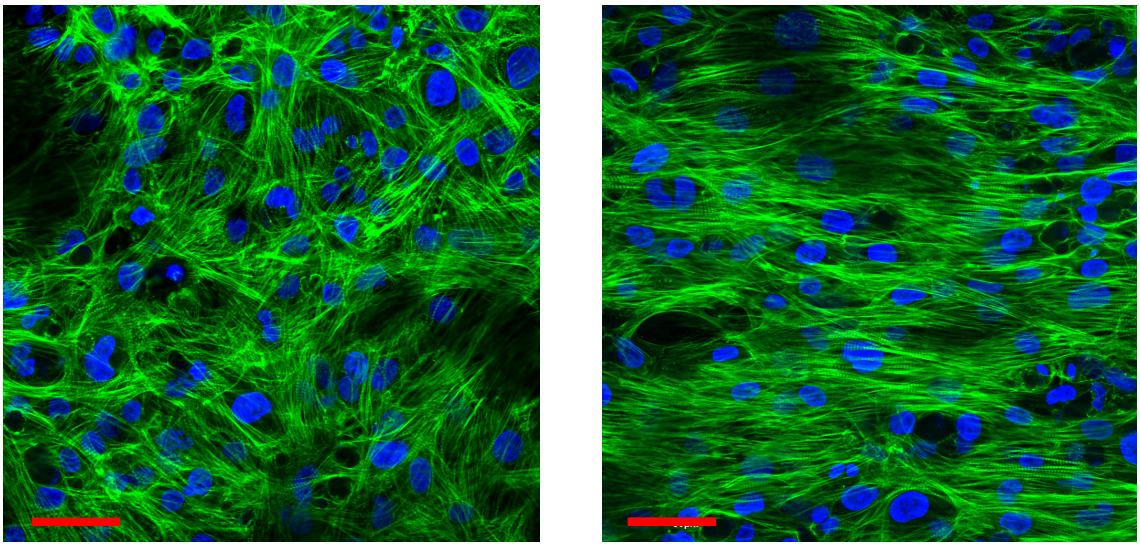

Control **MFG**

Scale bar = 50μm

Green; F-actin, Blue; DAPI

The images of the same sample in Figure 2I were obtained with 40x oil immersion objective lense.

Supplementary data 3. Intracellular structure of non-aligned or aligned cardiac tissue with confocal images on day 43

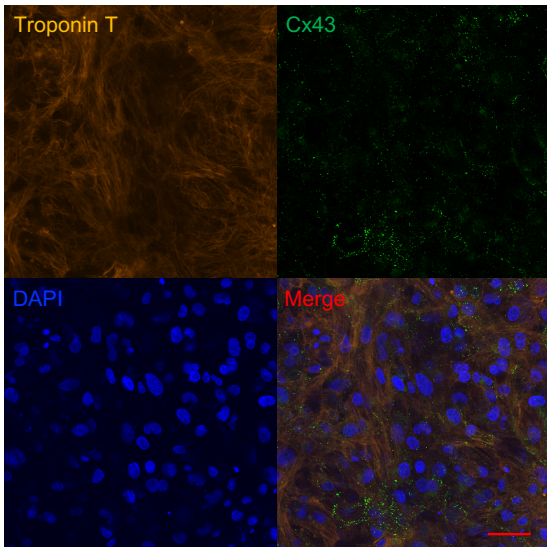

Non-aligned

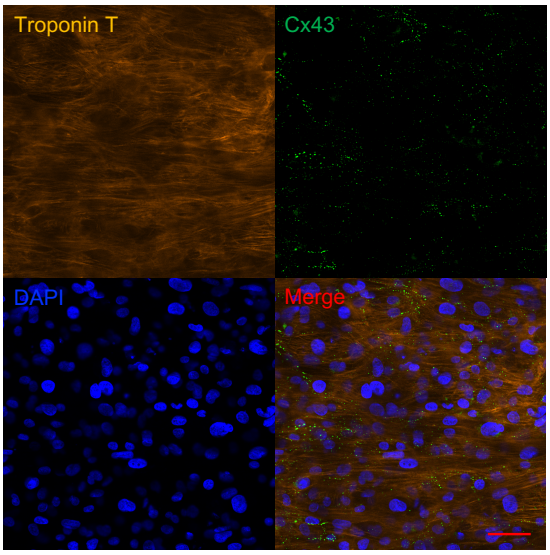

Aligned

Scale bar = 50μm

Supplementary data 4. Gene expression levels in non-aligned and aligned cardiac tissue on day 44

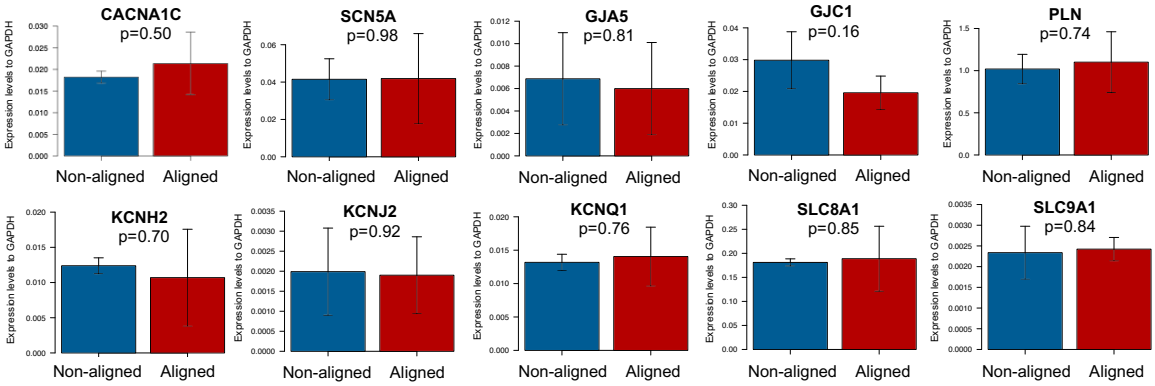

The number of experiments were three times (N=3).

Supplementary data 5. PIV analysis of aligned and non-aligned cardiac tissue

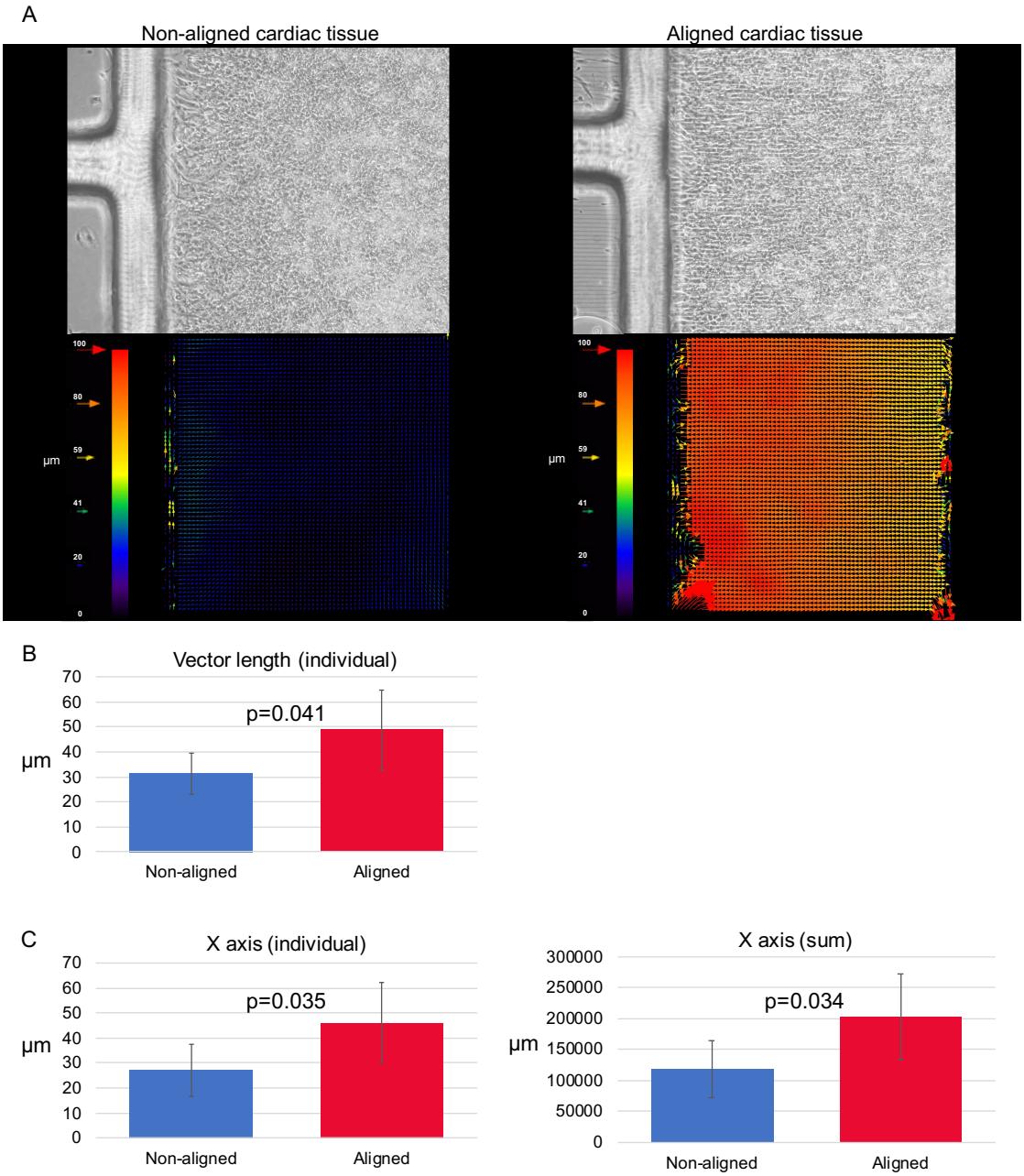

(A) Representative image of PIV analysis on day 43. (B) Vector length of each site. (C) X-axis components of an individual vector (left) and the sum of the X-axis component of vector length at each site (right) (N=6). PIV; particle image velocimetry